

# Understanding Selectivities in Ligand-free Oxidative Cyclizations of 1,5- and 1,6-Dienes with RuO<sub>4</sub> from Density Functional Theory

Philipp J. di Dio<sup>a</sup>, Stefan Zahn<sup>a</sup>, Christian B. W. Stark<sup>b</sup>, and Barbara Kirchner<sup>a</sup>

<sup>a</sup> Wilhelm-Ostwald-Institut für Physikalische und Theoretische Chemie, Universität Leipzig,  
Linnéstraße 2, 04103 Leipzig, Germany

<sup>b</sup> Institut für Organische Chemie, Universität Leipzig, Johannisallee 29, 04103 Leipzig, Germany

Reprint requests to B. Kirchner. E-mail: b.kirchner@uni-leipzig.de

Z. Naturforsch. **2010**, 65b, 367 – 375; received November 20, 2009

Dedicated to Professor Rolf W. Saalfrank on the occasion of his 70<sup>th</sup> birthday

Quantum-chemical calculations using density functional theory were carried out to investigate the mechanism of the oxidative cyclization of 1,5- and 1,6-dienes with ruthenium tetroxide. Current experimental results show different selectivities for the formation of tetrahydrofuran and tetrahydropyran derivatives. Our theoretical data correctly reproduce the experimental selectivities. Transition structures for the first [3+2]-cycloaddition of RuO<sub>4</sub> with ethene and for the second [3+2]-cycloaddition with two ethene molecules, 1,5-hexadiene, and 1,6-heptadiene were calculated. For the formation of tetrahydrofuran and tetrahydropyran derivatives we observed two reaction pathways. The transition structure for the formation of *cis*-tetrahydrofuran derivatives was found to be more stable than the *trans*-tetrahydrofuran-forming transition structure by about 40 kJ mol<sup>-1</sup>. By comparison to the reaction with two ethene molecules it was shown that the linking alkyl chain causes the energy gap between stereoisomers by a directing influence. In the tetrahydropyran reaction the *trans*-tetrahydropyran-forming transition structure was less than 4 kJ mol<sup>-1</sup> more stable than the transition structure leading to the *cis*-tetrahydropyran. The obtained geometries showed that for tetrahydropyrans the energy gap between stereoisomers is not caused by the linking alkyl chain.

Key words: Oxidative Cyclization, DFT, Cycloaddition

## Introduction

The direct oxidative diene cyclization has been known for some time [1]. Recently applications in total synthesis of natural products have been reported [2–8]. Especially *Annonaceous* acetogenins containing tetrahydrofuran (THF) and tetrahydropyran (THP) rings like membrarollin [9] are of special interest because of their antitumor activity [10]. A similar nitrogen-containing structural motif [11–13] appears in ligands for supramolecular chemistry synthesized by Saalfrank and co-workers [14, 15], see Fig. 1. The oxidative cyclization paves the way for simple diastereoselective synthesis of the oxygen analogous ligands for supramolecular chemistry.

In the oxidative cyclization as in *cis*-dihydroxylations the first step is a [3+2]-cycloaddition of MnO<sub>4</sub><sup>-</sup>, OsO<sub>4</sub>, or RuO<sub>4</sub> to a carbon-carbon double bond. The first dihydroxylation with MnO<sub>4</sub><sup>-</sup> was published by Hazura in 1888 [16]. He reported the oxidation of several unsaturated fatty acids by alkaline potassium per-

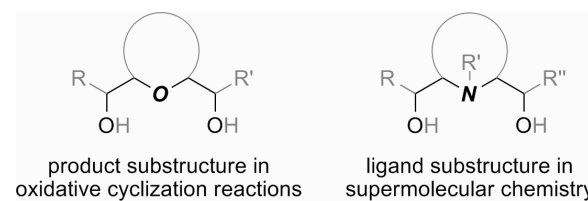


Fig. 1. Substructures of oxidative cyclization products and supramolecular chemistry ligands.

manganate solutions leading to dihydroxy fatty acids. Later a similar reaction with osmium tetroxide was observed. In 1912 Hofmann showed the catalytic effect of OsO<sub>4</sub> in the presence of co-oxidants like chlorates [17–19]. X-Ray crystal structures of several oxoosmium esters [20–22] and quantum chemical calculations [23–25] confirmed the proposed [3+2]-cycloaddition mechanism. Hydrolysis of these esters leads to *cis*-diols, the experimentally observed products. In 1953 Djerassi found the same reaction to occur with ruthenium tetroxide instead of OsO<sub>4</sub> or

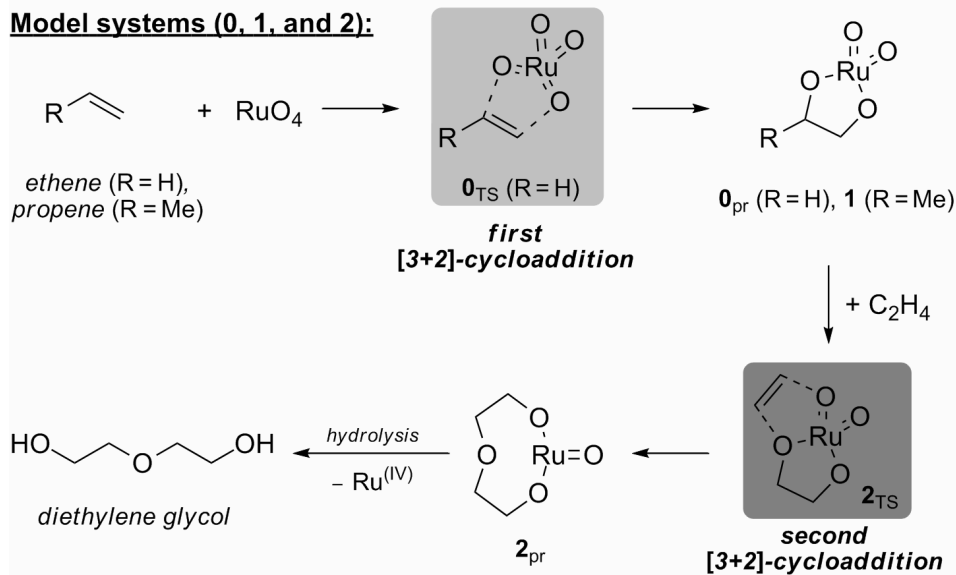
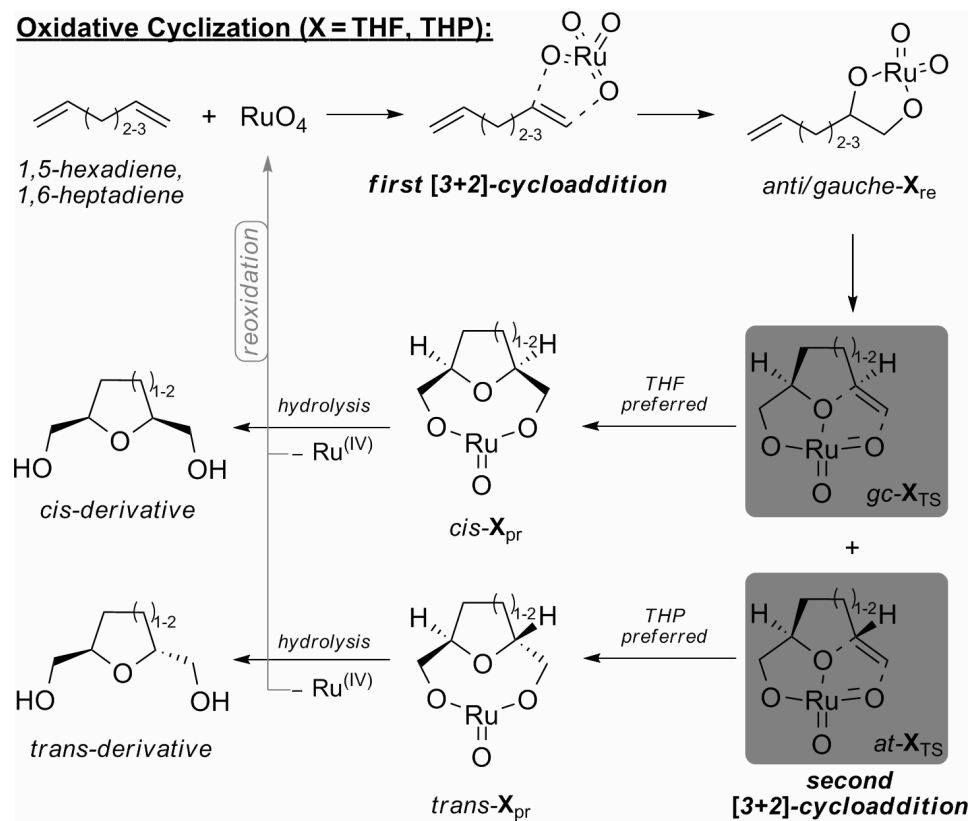


Fig. 2. Reaction mechanism of the oxidative cyclization with the first and second [3+2]-cycloaddition, investigated (model) systems, and their abbreviations.

$\text{MnO}_4^-$  following the same [3+2] mechanism [26–28]. Several detailed reviews of selectivities, reactivities, and applications of  $\text{OsO}_4$ ,  $\text{MnO}_4^-$ , and  $\text{RuO}_4$  in *cis*-dihydroxylations have been published [29–32].

Surprisingly, application of *cis*-dihydroxylation conditions to 1,5- and 1,6-dienes often led to cyclic ethers instead of the expected tetroles (Fig. 2). In 1895 the first oxidative cyclization was carried out by Tiemann and Semmler during structural investigations of geraniol and linalool with potassium permanganate. Unfortunately, it was impossible to isolate and identify the reaction products at the time [33]. Almost three decades later an envisaged double dihydroxylation of geranyl acetate led to the planned tetrole less one molecule of water, and an oxygen heterocycle was proposed by Kötz and Steche [34]. The product was identified as *cis*-dihydroxylinalool oxide by Klein and Röjahn [35]. They proposed a second ring closing [3+2]-cycloaddition (Fig. 2). The same product was formed with the use of  $\text{RuO}_4$  [36]. Several experimental results support the mechanism of a second, ring closing [3+2]-cycloaddition [35–40], especially reactions with  $^2\text{H}$ -labeled 1,5-hexadienes by Baldwin *et al.* [39]. The mechanism of the interaction between  $\text{MnO}_4^-$  and *trans-trans*-2,6-octadiene was calculated in 2007 [41].

Generally, it is noteworthy that reactions with 1,5-dienes yield *cis*-THF derivatives, while oxidative cyclization of 1,6-dienes produces *trans*-THP derivatives. High diastereoselectivities were observed with both substrate classes using  $\text{RuO}_4$ , and optimized procedures have been developed yielding a broad range of *cis*-THF and *trans*-THP derivatives [42–45].

In order to gain a deeper understanding of the reaction mechanism and the origin of the stereoselectivity, we investigated the transition structures for the ring closing reaction, highlighted in Fig. 2.

After a short section introducing the employed theoretical methods we present the results of our investigation. We first show the initial step in the oxidative cyclization reaction: the [3+2]-cycloaddition of  $\text{RuO}_4$  to a carbon-carbon double bond. Next, we compare the intermediates followed by a discussion of the second reaction step, see Fig. 2, which is responsible for the observed stereoselectivity. Finally, we give a short summary of our results.

## Computational Details

The program package TURBOMOLE 5.10 [46] was used to optimize all structures reported in this pa-

per. We used the BP86 [47, 48] functional where the RI approximation can be employed [49–51]. Furthermore, calculations employing the B3LYP functional are shown [48, 52, 53]. All calculations were carried out with the def2-TZVPP [54] basis set which includes a relativistic electron core potential for ruthenium [55], and the convergency criterion was increased to  $10^{-8}$  Hartree. For frequency calculations SNF 4.0 was chosen [56].

The investigation of the intermediates shows that the low-spin state is preferred compared to the high-spin state for the BP86 as well as the B3LYP functional (see Supporting Information). B3LYP underestimates the stability of the low-spin state due to a too large amount of exact Hartree Fock exchange (see the excellent works of Reiher *et al.* [57, 58]). Therefore, only the low-spin state must be considered which is presented in this work. Results for the high-spin state are included in the Supporting Information.

## Results and Discussion

Besides the oxidative cyclization of 1,5- and 1,6-dienes to THF and THP derivatives, respectively, we selected simpler model systems **0**, **1**, and **2** (see Fig. 2), because there we are able to distinguish between different contributions leading to the observed selectivities. Model system **0** consists of  $\text{RuO}_4$  and one ethene molecule and is investigated to gain structural and energetic informations about the first [3+2]-cycloaddition. Model system **1** is the product of  $\text{RuO}_4$  and propene and gives conformational insights into substituted oxoruthenium(VI) esters, because the methyl group is the pendant to the larger alkyl chains in the THF and THP reactions and should behave in a similar way as the alkyl chains do. The reaction of another ethene molecule with **0<sub>pr</sub>** is the model system **2** which represents the crucial step, the second [3+2]-cycloaddition. System **2** is free of a linking alkyl chain and therefore, the directing influence of this part on the reaction can be excluded. Comparing structural details of **2<sub>TS</sub>** with **THF<sub>TS</sub>/THP<sub>TS</sub>** allows us to determine the role of the alkyl chain on the selectivity of the oxidative cyclization. For a better overview all results are listed in Tables 1 and 2.

### [3+2]-Cycloaddition of $\text{RuO}_4$ to carbon-carbon double bonds

The first step in oxidative cyclizations is a [3+2]-cycloaddition of  $\text{RuO}_4$  to a carbon-carbon double bond

Table 1. Zero point energy corrected energy  $E_X^{\text{ZPE}}$  and free reaction enthalpy  $\Delta G_X$  at  $T = 298.15 \text{ K}$  in  $\text{kJ mol}^{-1}$  for all investigated compounds.

Structure	$E_{\text{BP86}}^{\text{ZPE}}$	$E_{\text{B3LYP}}^{\text{ZPE}}$	$\Delta G_{\text{BP86}}$	$\Delta G_{\text{B3LYP}}$
<b>0<sub>re</sub></b>	0	0	0	0
<b>0<sub>TS</sub></b>	11.1	18.7	65.9	73.6
<b>0<sub>pr</sub></b>	-107.1	-169.7	-53.5	-115.0
<b>anti-1</b>	0	0	0	0
<b>1<sub>TS</sub></b>	8.6	9.4	13.2	8.5
<b>gauche-1</b>	4.3	4.5	4.5	4.8
<b>2<sub>re</sub></b>	0	0	0	0
<b>2<sub>TS</sub></b>	87.4	101.5	143.5	156.2
<b>2<sub>pr</sub></b>	16.9	-33.1	70.7	19.5
<b>anti-THF<sub>re</sub></b>	0	0	0	0
<b>gauche-THF<sub>re</sub></b>	3.9	1.6	4.3	-1.4
<b>at-THF<sub>TS</sub></b>	117.0	132.9	127.6	140.1
<b>gc-THF<sub>TS</sub></b>	78.5	90.5	88.4	97.0
<b>cis-THF<sub>pr</sub></b>	12.9	-38.1	18.8	-34.9
<b>trans-THF<sub>pr</sub></b>	81.4	38.0	87.8	41.4
<b>anti-THP<sub>re</sub></b>	0	0	0	0
<b>gauche-THP<sub>re</sub></b>	3.6	0.2	4.7	-2.4
<b>at-THP<sub>TS</sub></b>	98.5	109.7	111.5	116.8
<b>gc-THP<sub>TS</sub></b>	101.7	113.1	114.7	120.4
<b>cis-THP<sub>pr</sub></b>	15.3	-38.8	25.6	-34.2
<b>trans-THP<sub>pr</sub></b>	25.8	-25.3	36.0	-20.2

Table 2. Bond lengths  $d_1$  and  $d_2$  in pm between oxygen and carbon for BP86 and B3LYP transition structures (illustrations of  $d_1$  and  $d_2$  can be seen in Fig. 3a for **0<sub>TS</sub>** and in Fig. 5a for all other structures).

Structure	$d_1$ (pm)		$d_2$ (pm)	
	BP86	B3LYP	BP86	B3LYP
<b>0<sub>TS</sub></b>	214	217	214	217
<b>2<sub>TS</sub></b>	174	180	205	210
<b>gc-THF<sub>TS</sub></b>	174	182	212	216
<b>at-THF<sub>TS</sub></b>	188	196	192	196
<b>gc-THP<sub>TS</sub></b>	175	182	213	217
<b>at-THP<sub>TS</sub></b>	178	185	207	211

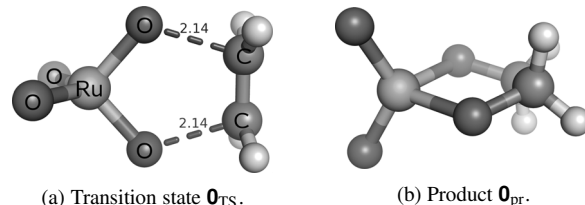


Fig. 3. [3+2]-Cycloaddition **0** of  $\text{RuO}_4$  to ethylene.

leading to oxoruthenium(VI) esters, see **0<sub>TS</sub>** and **0<sub>pr</sub>** in Fig. 3, and Fig. 2 for the reaction equation. Norrby *et al.* have already investigated this reaction with DFT approaches in 1994 [27]. We recalculated this reaction with a larger basis set for a better comparison of the energy barriers of the first and second [3+2]-cycloadditions.

The C-O-bond length is about 20 pm shorter compared to the results of Norrby *et al.* (233 pm) [27] (Table 2). The energy barrier was found to be  $\Delta G_{\text{BP86}} = 65.9 \text{ kJ mol}^{-1}$  /  $\Delta G_{\text{B3LYP}} = 73.6 \text{ kJ mol}^{-1}$ , significantly below the lowest energy barrier for the second reaction step from **0<sub>pr</sub>** to **2<sub>pr</sub>** of about 90  $\text{kJ mol}^{-1}$  (Fig. 2). Therefore, the second reaction step is rate-determining. The first [3+2]-addition is highly exergonic ( $\Delta G_{\text{BP86}} = -53.5$ ,  $\Delta G_{\text{B3LYP}} = -115.0 \text{ kJ mol}^{-1}$ ), in contrast to the subsequent ring closing reaction.

#### Anti-gauche equilibrium of intermediates

[3+2]-Cycloaddition of  $\text{RuO}_4$  to propene leads to 4-methyl-2,2-dioxo-2,1,3-ruthena(VI)dioxolane **1** (Figs. 2 and 4). We found that **1** and the esters formed with longer side chains exist in two conformations, an *anti*- and a *gauche*-conformer (Fig. 4). Our BP86 calculations predict that the *anti*-conformer is more stable than the *gauche*-conformer for all structures **1**, **THF<sub>re</sub>**, and **THP<sub>re</sub>** (Table 1). The B3LYP functional predicts the same for **1**. For the **THF<sub>re</sub>** and **THP<sub>re</sub>** structures, the B3LYP functional predicts the *gauche*-conformer to be more stable in contrast to **1** (Table 1).

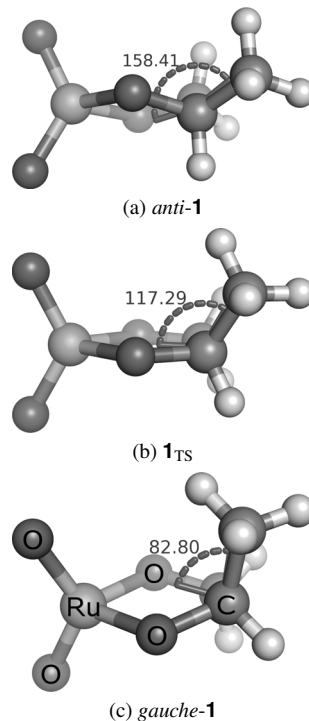


Fig. 4. Conformers of 3-methylruthenium(VI)dioxo-2,5-dioxolane **1** (BP86) with its transition state including torsion angles.

However, the energy gap between the two possible conformers is very small, and therefore the prediction of the most stable conformer is very sensitive to errors of the employed approaches. The enthalpy  $G$  depends on the entropy whose vibrational contribution  $S_{\text{vib}}$  is given by

$$S_{\text{vib}} = R \cdot \sum_i \left[ \frac{h\nu_i}{kT(e^{h\nu_i/kT} - 1)} - \ln \left( 1 - e^{-\frac{h\nu_i}{kT}} \right) \right]. \quad (1)$$

According to Eq. 1 ( $R$  = molar gas constant,  $k$  = Boltzmann constant,  $T$  = temperature,  $h$  = Planck constant, and  $\nu_i$  = vibrational frequencies), the maximum contribution to the entropy comes from vibrations with small frequencies. If a frequency  $\nu_i$  is very small and even tends to zero, then the fraction in Eq. 1 tends to one. Despite the fraction the logarithmic part in Eq. 1 tends to plus infinity when a frequency  $\nu_i$  tends to zero. Therefore the absolute slope of the vibrational contributions  $S_{\text{vib}}(\nu_i)$  as a function of the frequency  $\nu_i$  is very high for small frequencies and is even arbitrarily high for an arbitrarily small  $\nu_i$ .

Previous investigations by Reiher and co-workers have shown that the calculated values of frequencies with small wavenumbers are inaccurate to predict the spin-flip temperature of transition metal complexes [59]. Because of the large slope in  $S_{\text{vib}}(\nu_i)$  for small frequencies  $\nu_i$ , small deviations of calculated from experimental frequencies result in huge errors which can be as large as the energy gap between both conformers. Therefore, the assignment of the most stable conformer including  $S_{\text{vib}}$  should be treated with care.

Nevertheless, the energy barrier between both conformations is very small (Table 1). Therefore, the *anti-gauche* equilibrium of the intermediates should not substantially affect the reaction rates of the second reaction step.

#### Oxidative cyclization mechanism

Four reaction pathways are possible, due to two possible conformations in the intermediates (*anti-* and *gauche-X<sub>re</sub>*) and two product configurations (*cis-* and *trans-X<sub>pr</sub>*) (Fig. 2). Our investigations have revealed that only two pathways per reaction are reasonable. These are the *anti-trans-* (*at*) and the *gauche-cis*-reaction path (*gc*). The *at*- and *gc*- $\mathbf{X}_{\text{TS}}$  structures are highlighted in Fig. 2. The two other possible reaction paths either have a much higher energy barrier or lead directly via the *anti-gauche* equilibrium barrier,

*i.e.* constructing a *gauche-trans*-THF transition structure gave an enormous distortion in the alkyl chain and an energy barrier of more than 40 kJ mol<sup>-1</sup> higher than for the corresponding *anti-trans*-THF transition structure *at*- $\mathbf{THF}_{\text{TS}}$ . Furthermore, the construction of an *anti-cis*-THF transition structure resulted in a structure which has a torsion angle close to the *anti-gauche*-transition torsion angle of  $\mathbf{1}_{\text{TS}}$  (Fig. 4b). The structure has two negative frequencies, the smaller corresponding to the *anti-gauche*-transition.

The conformational differences can be gathered from Figs. 6 and 7, and especially from Fig. 4. For a better understanding, Newman projections of the THF transition states *at*- and *gc*- $\mathbf{THF}_{\text{TS}}$  are given in Fig. 6b.

#### Model structure 2 without a linking alkyl chain

The transition state of a simplified reaction without the connecting alkyl chain is shown in Fig. 5a. The definitions of the bond length  $d_1$  and  $d_2$  are also given in Fig. 5a and will be kept throughout the article. The bond lengths in  $\mathbf{2}_{\text{TS}}$  are 174 pm ( $d_1$ ) and 205 pm ( $d_2$ ) for BP86. Slightly larger lengths are obtained by the B3LYP calculations (second line Table 2).

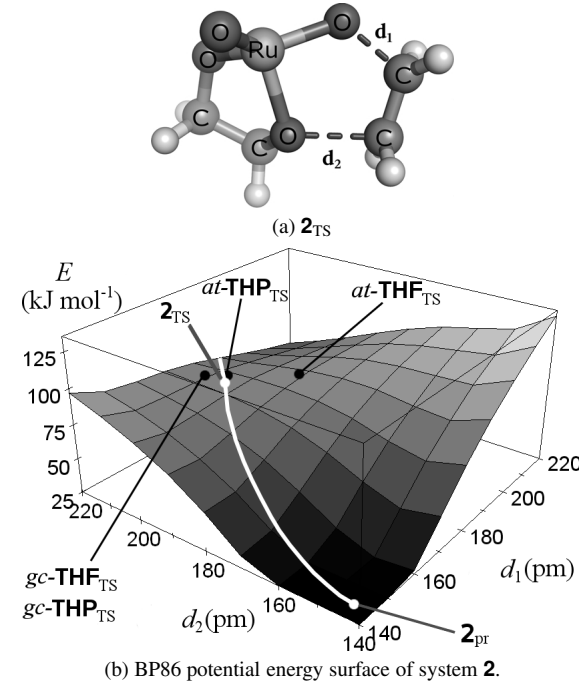


Fig. 5. (a): Transition state  $\mathbf{2}_{\text{TS}}$  of the reaction of ethene with ruthenium(VI)dioxo-2,5-dioxolane with bond lengths  $d_1$  and  $d_2$ ; (b): BP86 potential energy surface with BP86 THF/THP  $d_1$  and  $d_2$  data.

Structure **2<sub>TS</sub>** represents the transition state free of the directing influence of a linking alkyl chain. The other transition states **THF<sub>TS</sub>** and **THP<sub>TS</sub>** including the linking alkyl chain are compared to this structure and its distances  $d_1$  and  $d_2$  to gain informations about the influence of the alkyl chain. The corresponding potential energy surface leading to **2<sub>TS</sub>** illustrates that only one transition state can be found (Fig. 5b). All distances of the THF and THP transition states are included to demonstrate the scale of deviation in the bond lengths  $d_1$  and  $d_2$ .

#### THF transition structures: **THF<sub>TS</sub>**

The transition states for the second reaction step in the oxidative cyclization of 1,5-hexadiene are shown in Fig. 6. The distances  $d_1$ ,  $d_2$ , and relative ener-

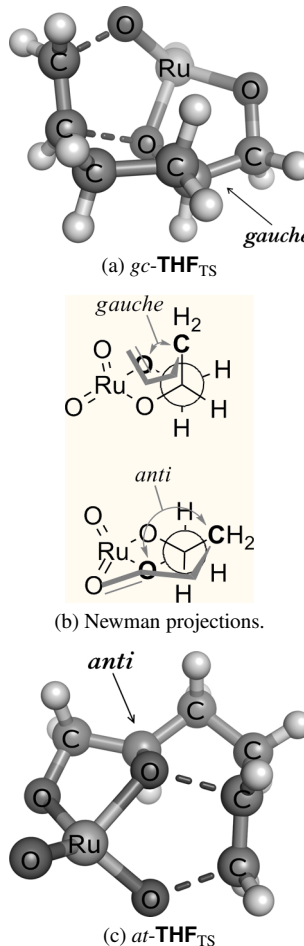


Fig. 6. THF transition states (a) *gauche-cis*-conformer; (b) Newman projections of a and c; (c) *anti-trans*-conformer. Some atoms are labeled to clarify the structures.

gies for *gc*-**THF<sub>TS</sub>** and *at*-**THF<sub>TS</sub>** are summarized in Tables 1 and 2. We found that the deviations of  $d_1$  and  $d_2$  from the model system **2<sub>TS</sub>** in *gc*-**THF<sub>TS</sub>** are small. Only  $d_2$  is slightly longer. In *at*-**THF<sub>TS</sub>** both distances are highly distorted compared to **2<sub>TS</sub>**.  $d_1$  is 14 pm longer and  $d_2$  13 pm shorter than in **2<sub>TS</sub>** for the BP86 structure. The B3LYP functional even shows a larger distance deviation for *at*-**THF<sub>TS</sub>** as compared to **2<sub>TS</sub>** of more than 15 pm with similar trends.

The linking alkyl chain causes the distortions and hence selects *gc*-**THF<sub>TS</sub>** as the preferred pathway. *gc*-**THF<sub>TS</sub>** leads to the formation of the *cis*-product in agreement with experimental data (Fig. 2). Therefore, we can conclude that in case of the reaction of 1,5-dienes with RuO<sub>4</sub> *cis*-selectivity is caused by the directing influence of the linking alkyl chain, destabilizing the transition state of the pathway to the *trans*-product.

The reaction profile with the  $\Delta G_{\text{B3LYP}}$  energies of all reactants, transition states, and products is shown in Fig. 8a. It summarizes the two reaction pathways via the *anti-trans*- and *gauche-cis*-transition structure. At first the *anti-gauche*-equilibrium is shown, and the transition energy for the conformational change is taken from the **1<sub>TS</sub>** structure. Furthermore, the energy barrier for the second [3+2]-cycloaddition is given for both pathways. The large energy gap demonstrates the selectivity between these two transition states. The product energies are very different with the thermodynamically more stable product being preferred. The very last step, the hydrolysis of **THF<sub>pr</sub>** (and **THP<sub>pr</sub>**), was not calculated and is therefore omitted because the stereochemistry of the products is completely determined by the transition states and remains untouched during hydrolysis.

#### THP transition structures: **THP<sub>TS</sub>**

The transition states *at*-**THP<sub>TS</sub>** and *gc*-**THP<sub>TS</sub>** are shown in Fig. 7. Deviations of the bond length  $d_1$

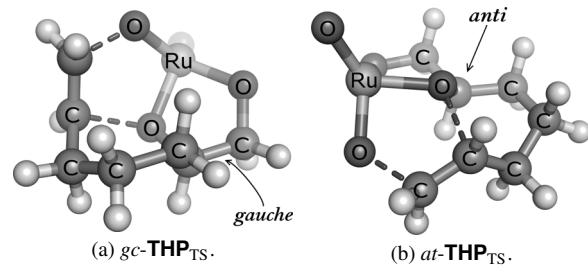


Fig. 7. THP transition states (a) *gauche-cis* and (b) *anti-trans*.

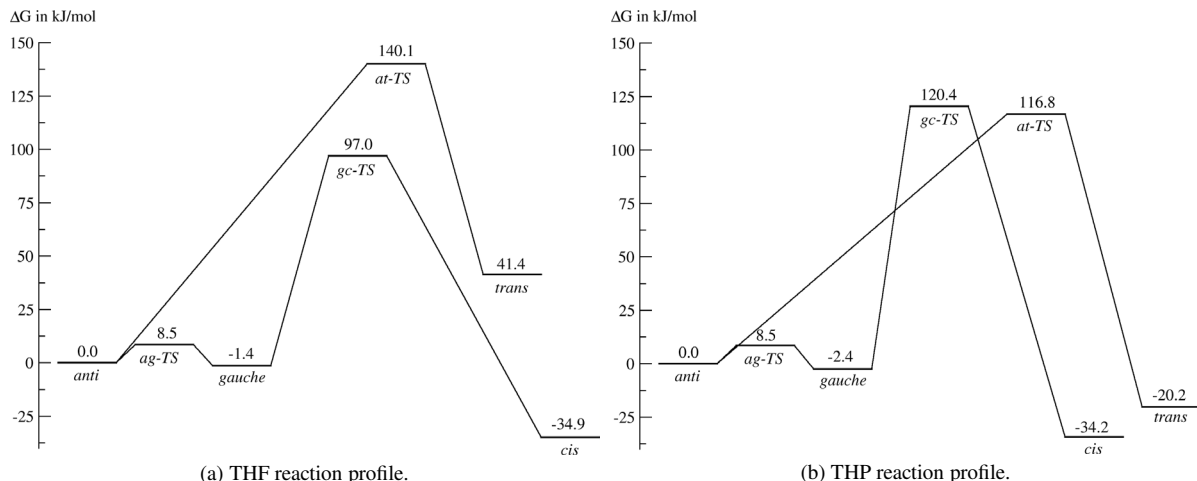


Fig. 8. Calculated  $\Delta G_{\text{B}3\text{LYP}}$  reaction profiles for the oxidative cyclization of 1,5-hexadiene and 1,6-heptadiene to *cis/trans*-THF and -THP derivatives.

and  $d_2$  compared to  $\mathbf{2}_{\text{TS}}$  are very small (Table 2 and Fig. 5b). Therefore, we conclude that the linking alkyl chain has no significant influence on *at*- $\mathbf{THP}_{\text{TS}}$  and *gc*- $\mathbf{THP}_{\text{TS}}$ . Furthermore, the small deviation in  $d_1$  and  $d_2$  in comparison to  $\mathbf{2}_{\text{TS}}$  confirms our calculated transition states. In the THF transition structures a large deviation of  $d_1$  and  $d_2$  in *at*- $\mathbf{THF}_{\text{TS}}$  in comparison to  $\mathbf{2}_{\text{TS}}$  compensates the strain of the alkyl chain. Because very little deviation is observed in the THP transition states, both alkyl chains are almost without strain, and none of the energy barriers is raised significantly. It should be noted that the energy gap between *at*- and *gc*- $\mathbf{THP}_{\text{TS}}$  is similar to the *anti-gauche* gap in the equilibrium of the intermediates.

The reaction profile is shown in Fig. 8b. It is similar to the THF reaction profile in Fig. 8a, but demonstrates the smaller energy gap between the two transition states as compared to the THF-system. Because the thermodynamically less stable *trans*-product is formed, it can be concluded that the reaction is not thermodynamically controlled. However, the energy gap we found is too small for a significant stereoselectivity.

## Conclusion

We calculated the transition states for the oxidative cyclization of 1,5-hexadiene and 1,6-heptadiene with  $\text{RuO}_4$  and compared the structures of the models with the simpler model systems **0**, **1** and **2** consisting of  $\text{RuO}_4$  and one ethene molecule, one propene molecule and two ethene molecules, respectively.

Our calculations showed that the mechanism proposed on the basis of the experiment and the calculated mechanism coincide with respect to the experimental *cis*-selectivity in case of THF derivative formation. The energy gap in the THP transition structures is too small for a significant assignment of *trans*-selectivity.

We found that the first [3+2]-cycloaddition leads to cyclic oxoruthenium esters coexisting in an *anti*- and a *gauche*-conformation. The energy barrier for interconversion of these conformers was calculated for a simpler model system **1** to be less than 14  $\text{kJ mol}^{-1}$ .

For the second [3+2]-cycloaddition we investigated a model system **2** without a linking alkyl chain. Two pathways from the *anti*-reactants leading to the *trans*-products (*at*-transition structure) and from *gauche*-reactants to *cis*-product (*gc*-transition structure) were detected. For the THF reaction we observed that the *gc*-transition structure is more stable than the *at*-transition structure by more than 39  $\text{kJ mol}^{-1}$ . Therefore, the experimentally found *cis*-selectivity for the THF formation is due to the more stable *gc*-transition structure as well as a more stable *cis* product. For the THP formation both transition structures are similar, and the *at*-transition structure is only 3–4  $\text{kJ mol}^{-1}$  more stable than the *gc*-structure.

The comparison of the THF and THP transition structures to our model system **2** lead to the conclusion that in the THF reaction the large energy gap between the *at*- and *gc*-structure is due to the directing influence of the linking alkyl chain. In the THP reaction the alkyl chain has no significant influence on the

transition structures and the energy gap. We noticed that the small energy gap in the THP transition structures is close to the energy gap between the *anti*- and *gauche*-reactant conformers, and that in both cases the *anti*-conformer is more stable.

#### Acknowledgement

This work was supported by the DFG, in particular by the project KI-768/6-1, and the ESF.

#### Supporting information

Further computational details including results for the high-spin state are contained in the Supporting Information available online.

- [1] V. Piccialli, *Synthesis* **2007**, *17*, 2585–2607.
- [2] A. R. Cecil, R. C. D. Brown, *Org. Lett.* **2002**, *4*, 3715–3718.
- [3] A. R. Cecil, Y. L. Hu, M. J. Vicent, R. Duncan, R. C. D. Brown, *J. Org. Chem.* **2004**, *69*, 3368–3374.
- [4] G. D. Head, W. G. Whittingham, R. C. D. Brown, *Synlett* **2004**, *8*, 1437–1439.
- [5] B. Lygo, D. Slack, C. Wilson, *Tetrahedron Lett.* **2005**, *46*, 6629–6632.
- [6] M. Friedel, G. Golz, P. Mayer, T. Lindel, *Tetrahedron Lett.* **2005**, *46*, 1623–1626.
- [7] T. J. Donohoe, R. M. Harris, J. Burrows, J. Parker, *J. Am. Chem. Soc.* **2006**, *128*, 13704–13705.
- [8] H. Göksel, C. B. W. Stark, *Org. Lett.* **2006**, *8*, 3433–3436.
- [9] C. L. Morris, Y. Hu, G. D. Head, L. J. Brown, W. G. Whittingham, R. C. D. Brown, *J. Org. Chem.* **2009**, *74*, 981–988.
- [10] A. Bermejo, B. Figadère, M.-C. Zafra-Polo, I. Barrachina, E. Esternell, D. Cortes, *Nat. Prod. Rep.* **2005**, *22*, 269–303.
- [11] T. J. Donohoe, G. W. Churchill, K. M. P. Wheelhouse, P. A. Glossop, *Angew. Chem.* **2006**, *118*, 8193–8196; *Angew. Chem. Int. Ed.* **2006**, *45*, 8025–8028.
- [12] T. J. Donohoe, K. M. P. Wheelhouse, P. J. Lindsay-Scott, P. A. Glossop, I. A. Nash, J. S. Parker, *Angew. Chem.* **2008**, *120*, 2914–2917; *Angew. Chem. Int. Ed.* **2008**, *47*, 2872–2875.
- [13] T. J. Donohoe, K. M. P. Wheelhouse, P. J. Lindsay-Scott, G. H. Churchill, M. J. Connolly, S. Butterworth, P. A. Glossop, *Chem. Asian J.* **2009**, *4*, 1237–1247.
- [14] R. W. Saalfrank, A. Scheurer, R. Prakash, F. W. Heinemann, T. Nakajima, F. Hampel, R. Leppin, B. Pilawa, H. Rupp, P. Müller, *Inorg. Chem.* **2007**, *46*, 1586–1592.
- [15] R. Puchta, V. Seitz, N. J. R. van Eikema Hommes, R. W. Saalfrank, *J. Mol. Model.* **2000**, *6*, 126–132.
- [16] K. Hazura, *Monatsh. Chem.* **1888**, *9*, 469–474.
- [17] K. A. Hofmann, *Ber. Dtsch. Chem. Ges.* **1912**, *45*, 3329–3336.
- [18] K. A. Hofmann, O. Ehrhart, O. Schneider, *Ber. Dtsch. Chem. Ges.* **1913**, *46*, 1657–1668.
- [19] R. Criegee, *Liebigs Ann. Chem.* **1936**, *522*, 75–96.
- [20] R. J. Collin, J. Jones, W. P. Griffith, *J. Chem. Soc., Dalton Trans.* **1974**, 1094–1097.
- [21] F. L. Phillips, A. C. Szapski, *J. Chem. Soc., Dalton Trans.* **1975**, 2586–2590.
- [22] L. G. Marzilli, B. E. Hanson, T. J. Kistenmacher, L. A. Epps, *Inorg. Chem.* **1976**, *15*, 1661–1665.
- [23] K. A. Jørgensen, R. Hoffmann, *J. Am. Chem. Soc.* **1986**, *108*, 1867–1876.
- [24] K. N. Houk, T. Strassner, *J. Org. Chem.* **1999**, *64*, 800–802.
- [25] P. Gisdakis, N. Rösch, *J. Am. Chem. Soc.* **2001**, *123*, 697–701.
- [26] C. Djerassi, R. R. Engle, *J. Am. Chem. Soc.* **1953**, *75*, 3838–3840.
- [27] P.-O. Norrby, H. C. Kolb, K. B. Sharpless, *Organometallics* **1994**, *13*, 344–347.
- [28] J. Frunzke, C. Loschen, G. Frenking, *J. Am. Chem. Soc.* **2004**, *126*, 3642–3652.
- [29] M. B. Smith, J. March, *March's Advanced Organic Chemistry – Reactions, Mechanisms, and Structure*, Wiley-Interscience, Hoboken, New Jersey, **2007**, chapter 15–48.
- [30] B. Plietker, *Synthesis* **2005**, *15*, 2453–2472.
- [31] B. Plietker, *Eur. J. Org. Chem.* **2005**, 1919–1929.
- [32] C. H. Hövelmann, K. Muñiz, *Chem. Eur. J.* **2005**, *11*, 3951–3958.
- [33] F. Tiemann, F. W. Semmler, *Ber. Dtsch. Chem. Ges.* **1895**, *28*, 2126–2137.
- [34] A. Kötz, T. Steche, *J. Prakt. Chem.* **1924**, *107*, 193–210.
- [35] E. Klein, W. Rojahn, *Tetrahedron* **1965**, *21*, 2353–2358.
- [36] H. J. Carlsen, T. Katsuki, V. S. Martin, K. B. Sharpless, *J. Org. Chem.* **1981**, *46*, 3936–3938.
- [37] K. A. Powell, A. L. Hughes, H. Katchian, J. F. Jerauld, H. Z. Salbe, *Tetrahedron* **1972**, *28*, 2019–2027.
- [38] D. M. Walba, M. D. Wand, M. C. Wilkes, *J. Am. Chem. Soc.* **1979**, *101*, 4396–4397.
- [39] J. E. Baldwin, M. J. Crossley, E.-M. M. Lehtonen, *J. Chem. Soc., Chem. Comm.* **1979**, 918–920.
- [40] D. M. Walba, P. D. Edwards, *Tetrahedron Lett.* **1980**, *21*, 3531–3534.

- [41] A. Poething, T. Strassner, *Collect. Czech. Chem. Commun.* **2007**, *72*, 715–727.
- [42] L. Albarella, D. Musumeci, D. Sica, *Eur. J. Org. Chem.* **2001**, 997–1003.
- [43] V. Piccialli, N. Cavallo, *Tetrahedron Lett.* **2001**, *42*, 4695–4699.
- [44] S. Roth, S. Göhler, H. Cheng, C. B. W. Stark, *Eur. J. Org. Chem.* **2005**, 4109–4118.
- [45] S. Roth, C. B. W. Stark, *Angew. Chem.* **2006**, *118*, 6364–6367; *Angew. Chem. Int. Ed.* **2006**, *45*, 6218–6221.
- [46] R. Ahlrichs, M. Bär, M. Häser, H. Horn, C. Kölmel, *Chem. Phys. Lett.* **1989**, *162*, 165–169.
- [47] J. P. Perdew, *Phys. Rev. B* **1986**, *33*, 8822–8824.
- [48] A. D. Becke, *Phys. Rev. A* **1988**, *38*, 3098–3100.
- [49] E. J. Baerends, D. E. Ellis, P. Ros, *Chem. Phys.* **1973**, *2*, 41–51.
- [50] B. I. Dunlap, J. W. D. Connolly, J. R. Sabin, *J. Chem. Phys.* **1979**, *71*, 3396–3402.
- [51] F. Weigend, *Phys. Chem. Chem. Phys.* **2006**, *8*, 1057–1065.
- [52] C. Lee, W. Yang, R. G. Parr, *Phys. Rev. B* **1988**, *37*, 785–789.
- [53] A. D. Becke, *J. Chem. Phys.* **1993**, *98*, 5648–5652.
- [54] F. Weigend, R. Ahlrichs, *Phys. Chem. Chem. Phys.* **2005**, *7*, 3297–3305.
- [55] D. Andrae, U. Häußermann, M. Dolg, H. Stoll, H. Preuß, *Theor. Chim. Acta* **1990**, *77*, 123–141.
- [56] J. Neugebauer, M. Reiher, C. Kind, B. A. Hess, *J. Comput. Chem.* **2002**, *23*, 895–910.
- [57] M. Reiher, O. Salomon, B. A. Hess, *Theor. Chem. Acc.* **2001**, *107*, 48–55.
- [58] O. Salomon, M. Reiher, B. A. Hess, *J. Chem. Phys.* **2002**, *117*, 4729–4737.
- [59] G. Brehm, M. Reiher, S. Schneider, *J. Phys. Chem. A* **2002**, *106*, 12024–12034.

# **Understanding Selectivities in Ligand-free Oxidative Cyclization of 1,5- and 1,6-Dienes with RuO<sub>4</sub> from Density Functional Theory.**

*Supporting Information*

Philipp J. di Dio,<sup>a</sup> Stefan Zahn,<sup>a</sup> Christian B. W. Stark,<sup>b</sup>  
and Barbara Kirchner<sup>a,1</sup>

<sup>a</sup> Wilhelm-Ostwald-Institut für Physikalische und Theoretische Chemie,  
Universität Leipzig, Linnéstr. 2, D-04103 Leipzig, Germany

<sup>b</sup> Institut für Organische Chemie,  
Universität Leipzig, Johannisallee 29, D-04103 Leipzig, Germany

---

<sup>1</sup>bkirchner@uni-leipzig.de

## A High-spin BP86-Calculations

The program package TURBOMOLE 5.10 [1] was used to optimize all structures. We used the BP86 [2, 3] functional where the RI approximation can be employed [4–6]. Furthermore, single point calculations employing the B3LYP functional were performed for the BP86 structures [3, 7, 8]. All calculations were carried out with the def2-TZVPP [9] basis set including the relativistic def2-ecp for ruthenium [10] and the convergency criterion was increased to  $10^{-8}$  Hartree.

For  $\mathbf{2}_{\text{TS}2}$  and  $\mathbf{2}_{\text{pr}}$  we performed high-spin B3LYP optimizations and found that the corresponding low-spin B3LYP geometries are more stable. Because B3LYP overestimates the stability of high-spin states the low-spin reaction pathway is favoured.

In the following subsections we present the energies and structures for the high-spin states.

### A.1 Model system 2

In the high-spin state **2** we found two transition states and an intermediate, see Fig. A.

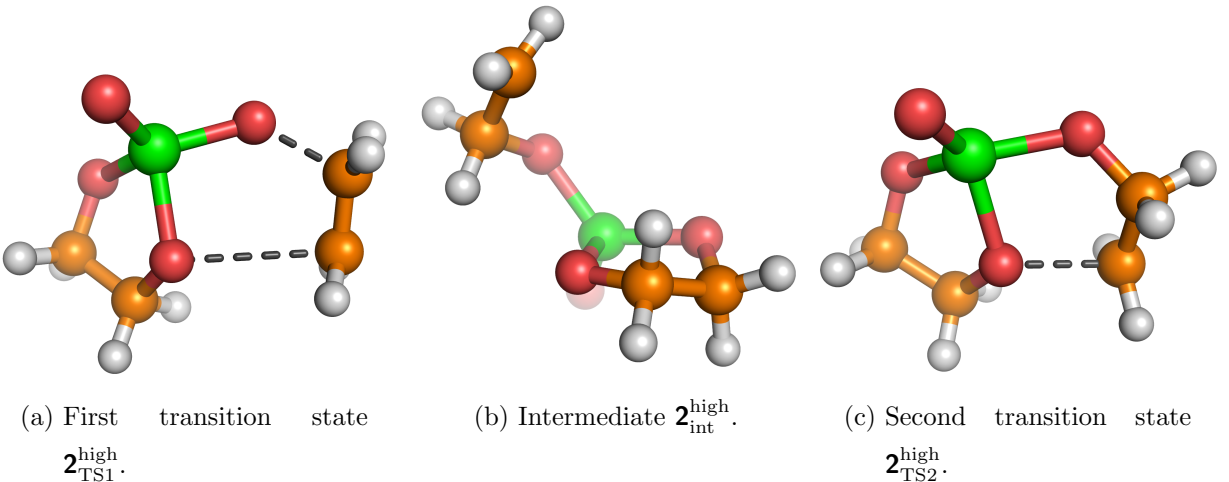


Fig. A. High-spin structures of model system **2**.

## A.2 High-spin potential energy surface of model system 2

The high-spin potential energy surface is shown for two views in Fig. B. The two transition states are marked. The coloured low-spin surface is shown in Fig. Ba.

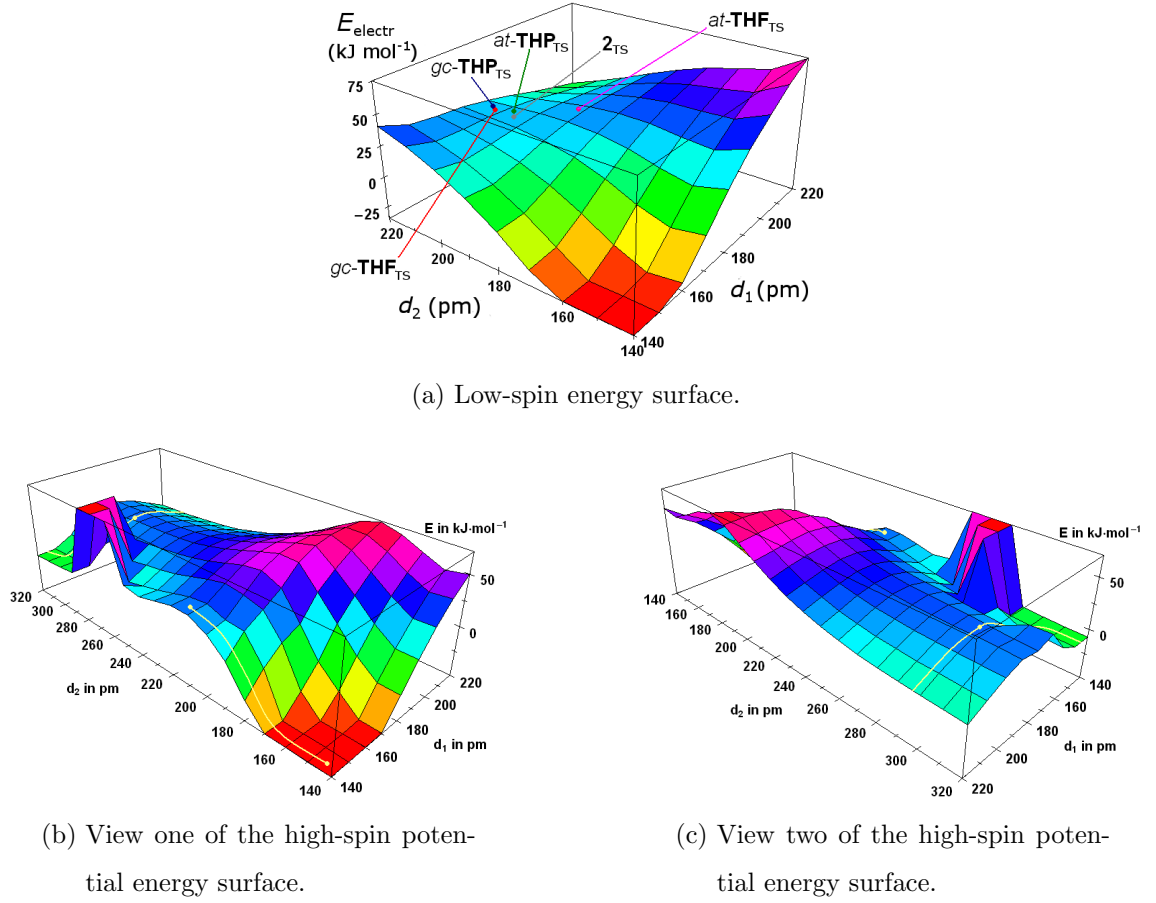


Fig. B. Low- and high-spin potential energy surfaces (BP86) of model system 2.

## A.3 High-spin THF transition structures

For the THF transition states we found similar structures compared to the low-spin, see Fig. C. We did not find an intermediate like  $\mathbf{2}_{\text{int}}^{\text{high}}$ .

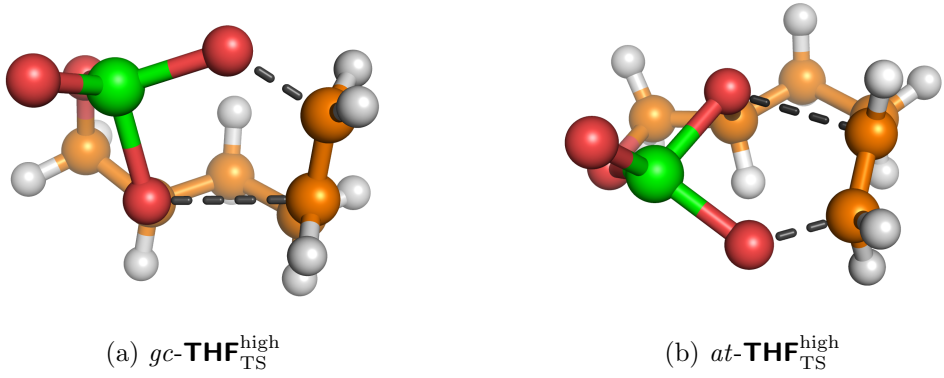


Fig. C. High-spin THF transition structures.

#### A.4 High-spin THP transition structures

In the THP high-spin reaction we found three transition structures similar to the low-spin structures and an intermediate, see Fig. D.

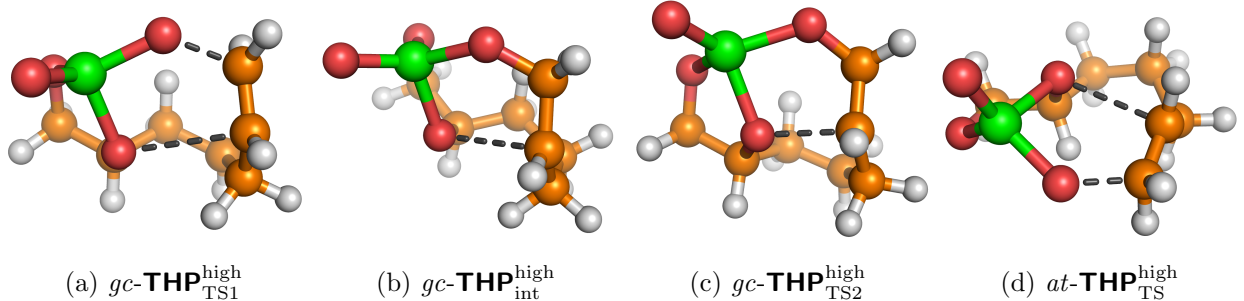


Fig. D. High spin THP transition structures and intermediate.

#### A.5 Electronic BP86 and B3LYP energies of the low- and high-spin THF and THP structures

In table A1 are all electronic BP86 and single point B3LYP energies of the presented structures shown relative to the structure  $anti\text{-}\mathbf{X}_{re}^{\text{low}}$ .

Table A1. BP86 and B3LYP energies [kJ mol<sup>-1</sup>] relative to *anti*- $\mathbf{X}_{\text{re}}^{\text{low}}$  for the THF and THP structures.

Geometrie	<b>X = THF</b>				<b>X = THP</b>			
	Z = low		Z = high		Z = low		Z = high	
	BP86	B3LYP	BP86	B3LYP	BP86	B3LYP	BP86	B3LYP
<i>anti</i> - $\mathbf{X}_{\text{re}}^{\text{Z}}$	0.0	0.0	76.9	70.1	0.0	0.0	76.3	69.0
<i>g</i> - $\mathbf{X}_{\text{re}}^{\text{Z}}$	2.5	3.4	79.9	73.8	2.7	3.4	79.8	69.0
<i>at</i> - $\mathbf{X}_{\text{TS}}^{\text{Z}}$	114.8	133.6	196.8	188.1	91.4	110.9	165.3	162.3
<i>gc</i> - $\mathbf{X}_{\text{TS}}^{\text{Z}}$	77.3	92.8	146.2	141.2	94.9	114.3	169.0	157.6
<i>gc</i> - $\mathbf{X}_{\text{int}}^{\text{Z}}$	—	—	—	—	—	—	145.0	120.2
<i>gc</i> - $\mathbf{X}_{\text{TS2}}^{\text{Z}}$	—	—	—	—	—	—	166.7	158.7
<i>trans</i> - $\mathbf{X}_{\text{pr}}^{\text{Z}}$	72.5	32.4	70.9	16.1	20.2	-33.8	39.4	-19.8
<i>cis</i> - $\mathbf{X}_{\text{pr}}^{\text{Z}}$	3.4	-44.7	22.0	-38.1	3.6	-46.3	23.7	-36.3

## A.6 High-spin bond distances

For the high-spin structures and the low-spin structures already presented in the paper the bond distances  $d_1$  and  $d_2$  are listed in table A2.

Table A2. Bond distances  $d_1$  and  $d_2$  of the high- and low-spin transition states for BP86 and B3LYP functional.

structure	BP86 low-spin		BP86 high-spin		B3LYP low-spin	
	$d_1$ [pm]	$d_2$ [pm]	$d_1$ [pm]	$d_2$ [pm]	$d_1$ [pm]	$d_2$ [pm]
<b>2<sub>TS</sub></b>	174	205	183	297	180	210
<b>2<sub>Int</sub></b>	—	—	147	352	—	—
<b>2<sub>TS2</sub></b>	—	—	144	213	—	—
<i>at</i> - <b>THF<sub>TS</sub></b>	188	192	169	242	196	196
<i>gc</i> - <b>THF<sub>TS</sub></b>	174	212	182	260	182	216
<i>at</i> - <b>THP<sub>TS</sub></b>	178	207	176	250	185	211
<i>gc</i> - <b>THP<sub>TS</sub></b>	175	213	182	287	182	217
<i>gc</i> - <b>THP<sub>int</sub></b>	—	—	148	286	—	—
<i>gc</i> - <b>THP<sub>TS2</sub></b>	—	—	146	215	—	—

## B Cartesian coordinates and total energy in a.u. of low-spin structures

The Cartesian coordinates and energies in a.u. of all low-spin structures are listed in table B1 to B20.

Table B1. Cartesian coordinates and total energy in a.u. for RI-BP86/TZVPP of  $\mathbf{0}_{\text{TS}}$ ,  
 $E(\text{RI-BP86/TZVPP}) = -474.6909783894$

O	-0.05493613938564	0.02920578659817	3.20369927228306
Ru	0.06580405137275	0.17180517835973	-0.06480246544755
O	-1.20046172858463	-2.47328123123778	-1.36207602711194
O	3.32557432596953	0.16262677553437	-0.36670787420946
O	-1.16172915588119	2.93797474245148	-1.12512530120890
C	5.34803705363333	0.00090617197458	3.14014073415945
C	3.56241029983366	-0.07316431123715	5.02613380887273
H	6.25693894609527	1.76920776813949	2.61701686489011
H	6.24101850913584	-1.72322121101516	2.46448495965064
H	3.00462957258842	-1.85766795662284	5.88116856753799
H	3.02225076854973	1.63469785117083	6.03508002367101

Table B2. Cartesian coordinates and total energy in a.u. for B3LYP/TZVPP of  $\mathbf{0}_{\text{TS}}$ ,  
 $E(\text{B3LYP/TZVPP}) = -474.2562419307$

O	-0.07077930409763	0.03128113252993	3.17065109704520
Ru	0.06127617830173	0.17211094730607	-0.06915780723300
O	-1.18448838850573	-2.45530616595982	-1.34634105022632
O	3.29173140843968	0.16390876287373	-0.38087982751997
O	-1.14705944010327	2.91791962310914	-1.11166735189065
C	5.35781519874139	-0.00008843826477	3.16066648750736
C	3.58341340637849	-0.07366612595427	5.03471903946689
H	6.24636814804235	1.75659145249369	2.62485945148226
H	6.22971614401313	-1.71148801004076	2.47267887180471
H	3.01173514468277	-1.84509274727242	5.87005217432819
H	3.02980800743418	1.62291913329519	6.02343147832249

Table B3. Cartesian coordinates and total energy in a.u. for RI-BP86/TZVPP of  $\mathbf{0}_{\text{pr}}$ ,  
 $E(\text{RI-BP86/TZVPP}) = -474.7364646902$

C	0.69585131591995	5.09934202758281	-0.25375279341456
C	0.84250217708737	4.70228059556043	2.56379855383926
H	2.59298466889718	5.21963343091875	-1.10328965850250
H	-0.96888498040615	5.14901413909051	3.48876246582996
H	2.36061230854956	5.78637308841069	3.47948381172813
H	-0.40410806035908	6.77524078642401	-0.80163963014560
O	-0.58574348941354	2.91512748521165	-1.31202378552226
O	1.39094747904618	2.04502784905334	2.97778683249013
Ru	0.01642290061855	-0.09246315635415	0.48905504532088
O	-2.70157714753869	-1.35724076325853	1.58091998471253
O	2.29524928671758	-1.76175338683208	-0.99362580758013

Table B4. Cartesian coordinates and total energy in a.u. for B3LYP/TZVPP of **0<sub>pr</sub>**,  
E(B3LYP/TZVPP)= -474.3280928952

C	0.66415110399406	4.73781148099128	-0.24468984870815
C	0.82432637159874	4.34825584258478	2.57269870871421
H	2.54483443369463	4.88023616920804	-1.08999279271584
H	-0.97019447998550	4.79592102500710	3.49536881653819
H	2.32899009422022	5.44506244311759	3.46058911164016
H	-0.43901431017784	6.39825775092796	-0.77471533084598
O	-0.58994781570345	2.55981577913228	-1.28889194986784
O	1.37888500024621	1.71689791114365	2.99138032804403
Ru	0.02183985422314	-0.42933914607896	0.51695393898750
O	-2.67926115648078	-1.65866841149827	1.59872249930578
O	2.30836311276600	-2.05353107596813	-0.93579727390790

Table B5. Cartesian coordinates and total energy in a.u. for RI-BP86/TZVPP of *anti-1*,  
E(RI-BP86/TZVPP)= -514.0458059483

C	1.65047740040157	1.22581350932698	0.17528029325407
C	1.96038002072171	0.59905151247058	2.94749316234091
C	4.04541156204834	1.99449434141813	-1.20512646855671
O	-0.15481609274068	-0.96731650106312	3.70208628588371
O	0.67254759284367	-1.06836794633687	-1.01932567649042
Ru	-1.37626596128707	-3.05386752666124	1.09307453785287
O	-0.16517373941259	-5.98419607298143	1.44907633318385
O	-4.43979367941935	-2.43926631000863	0.44753872880439
H	3.65222315930999	2.27183956216070	-3.22159055025947
H	4.77999095370599	3.77834148581639	-0.43780373391561
H	5.50603442212122	0.53364354889250	-1.01184114393512
H	0.17867128874190	2.68774922171633	-0.04661931650957
H	3.72298974091926	-0.46613200376011	3.27287740859397
H	1.94117135203500	2.27404704853999	4.17766542892779

Table B6. Cartesian coordinates and total energy in a.u. for B3LYP/TZVPP of *anti-1*,  
 $E(\text{B3LYP/TZVPP}) = -513.6074541170$

C	1.79388071222613	1.37825842976507	0.15545124546819
C	2.10646815599518	0.79365684453127	2.93531791649039
C	4.18994566668615	2.13512205362116	-1.21874833301523
O	0.00985847832916	-0.75080118263201	3.70796599160804
O	0.82084512923153	-0.90821287100697	-0.99727866403167
Ru	-1.21626922958807	-2.86185401336483	1.13814081353073
O	0.01228272417798	-5.74758642721715	1.51660430238279
O	-4.24777249529563	-2.23320060876140	0.51107985372030
H	3.80126022686600	2.42668852699569	-3.21948920955474
H	4.93509597134667	3.89489801622704	-0.44298112614378
H	5.62710927862989	0.66945865647967	-1.03723847748852
H	0.34270759484842	2.83593599753773	-0.08031102475001
H	3.86005461311830	-0.25165169044549	3.27378564220164
H	2.09163571309660	2.48245149868924	4.11962516934394

Table B7. Cartesian coordinates and total energy in a.u. for RI-BP86/TZVPP of **1**<sub>TS</sub>,  
 $E(\text{RI-BP86/TZVPP}) = -514.0407913381$

Ru	0.10736241311374	-0.00544579268648	-1.36154892592710
O	0.97795694444531	-1.72045640615185	1.59801240914269
O	2.51306300991225	1.87737442046459	-2.29226279081543
O	-1.48652754898405	-1.93347367324525	-3.34563409211930
O	-2.14862870857245	1.78234467112638	0.68915793442537
C	-0.28172319172468	-0.95666213808584	3.94293504822641
C	-2.22784710695174	1.08859690495846	3.34265335807255
H	-4.17042897355121	0.45761098379228	3.73641109164308
H	-1.87195600797898	2.83311049367525	4.42018340639745
C	1.74694584443293	-0.14781264060126	5.81640476821539
H	-1.22436244427802	-2.68555829482779	4.62163883134084
H	3.15770574477061	-1.64879457928748	6.04873090515391
H	2.70585275982060	1.57117675274088	5.15594067538740
H	0.89837396051270	0.24041209555022	7.67225898750010

Table B8. Cartesian coordinates and total energy in a.u. for B3LYP/TZVPP of **1<sub>TS</sub>**,  
 $E(\text{B3LYP/TZVPP}) = -513.6042068467$

Ru	0.12154641020117	-0.00352368904084	-1.35082166115390
O	0.97920600242942	-1.71463441040451	1.60403056025202
O	2.50062049529819	1.88234182778277	-2.23432154937355
O	-1.45989570408396	-1.92513873099714	-3.29929345276507
O	-2.13790687176920	1.77145869029315	0.68837799100033
C	-0.27779217076900	-0.96492076517812	3.92028785658893
C	-2.24473771598593	1.06423192927625	3.31138322729382
H	-4.16439319122699	0.40096633026284	3.68205374427914
H	-1.92644970998770	2.78414804639786	4.40919396708467
C	1.72128077294822	-0.13232849517251	5.80636015231191
H	-1.20938889776907	-2.67684912450146	4.60758750456687
H	3.12136409575243	-1.61909135469427	6.06863593202754
H	2.68090669188911	1.56903279165632	5.14517643411518
H	0.85324733562272	0.27209462750433	7.63415623819989

Table B9. Cartesian coordinates and total energy in a.u. for RI-BP86/TZVPP of *gauche-1*,  
 $E(\text{RI-BP86/TZVPP}) = -514.0440713106$

C	-0.57817475891915	1.70232546808655	-0.16358404483178
C	-0.36984750888278	0.67326279061311	2.51863549810488
C	2.31788117672935	0.24842468670545	3.41559980621852
O	3.15358411021241	-2.18855335527056	2.47210793051852
O	-1.61699307559130	-1.79366186996385	2.66266576959293
H	-1.42707956880834	1.88199910080605	3.84351984797722
Ru	0.53725081491178	-4.56969273557905	2.15302330901741
H	3.66121967626370	1.66227698104180	2.69620519959823
H	2.42219038499304	0.20881731044985	5.49423249769715
O	0.26879567476904	-5.59227569155582	-0.85974467471235
O	0.54935266589103	-6.48963135760381	4.70019211780970
H	0.13099152656973	3.65216527197368	-0.23794992495486
H	0.52578305207040	0.54749137831853	-1.48933387848546
H	-2.55648314292799	1.70257764930959	-0.78204254164325

Table B10. Cartesian coordinates and total energy in a.u. for B3LYP/TZVPP of *gauche-1*,  
 $E(\text{B3LYP/TZVPP}) = -513.6056388186$

C	-0.52500535181963	2.68004386736648	-0.60229210642353
C	-0.36905404759441	1.62023247040493	2.06583900019785
C	2.29835838313055	1.37302684209003	3.08271605418542
O	3.33490222199528	-0.97273525511397	2.17489558766868
O	-1.43823134478900	-0.90439536390911	2.12388487795476
H	-1.54517018119261	2.73989690337361	3.34321349083475
Ru	0.91536769850533	-3.51598887344594	1.71562851282538
H	3.55319511126146	2.88013610510122	2.44145956607261
H	2.30599421857406	1.33012630229389	5.14835795947557
O	0.88114474081978	-4.48065186422284	-1.29377946138197
O	0.92250158123366	-5.41232711159719	4.24130321916768
O	0.03780133878236	4.66403155429235	-0.61231404488413
O	0.71111074053784	1.64303973318630	-1.88610240743571
O	-2.45514769603630	2.54815146000178	-1.30701299002326

Table B11. Cartesian coordinates and total energy in a.u. for RI-BP86/TZVPP of **2<sub>TS</sub>**,  
 $E(\text{RI-BP86/TZVPP}) = -553.2749202790$

C	6.10695891057778	-2.89687994694873	6.16399352348861
O	4.58707722772883	0.66871578092591	6.08350929318998
C	1.83932718609222	0.62285945913687	6.49878505536354
C	0.82893529303840	2.95859417127013	5.19709363257529
O	2.01682508470766	3.06509851108413	2.73984768197268
Ru	5.49308072354503	2.21934020257769	2.89363129702291
O	7.45170809543941	4.72274504477244	2.74322212946043
C	6.86347540454646	-3.37549028477859	3.63703312841871
O	6.35387835130755	-0.80525832076076	1.66451979136434
H	-1.22903890044313	2.86153608738741	4.90137832517582
H	1.26842392334296	4.67865802084042	6.28722786027545
H	1.03429471940109	-1.08854045511665	5.63631937330125
H	1.51597085140245	0.59569829386152	8.55086888051634
H	4.40058483763413	-3.76470200720246	6.91516742509718
H	7.48327059344579	-2.26282557237333	7.55085658928836
H	8.89261131915261	-3.52897147407747	3.30792886025985
H	5.74623873521052	-4.74257728269482	2.57381824639516

Table B12. Cartesian coordinates and total energy in a.u. for B3LYP/TZVPP of **2<sub>TS</sub>**,  
 $E(\text{B3LYP/TZVPP}) = -552.8073690252$

C	6.12151916543804	-2.98269402101553	6.14343635170966
O	4.55710931820379	0.67066932023961	6.07395072184657
C	1.85043408075947	0.67143933139129	6.52187481357215
C	0.82543846478994	2.98092834228885	5.18216430929540
O	1.99794826430110	3.06463106009199	2.74709748690700
Ru	5.46408392006397	2.19648830888223	2.89266834623470
O	7.41108189931721	4.68016130474500	2.79421295188886
C	6.92747776455772	-3.44498560353823	3.66413606130713
O	6.28564569304058	-0.78308444710371	1.63159427490399
H	-1.21967963477935	2.86978743952942	4.90995556339482
H	1.25582925699623	4.70183888465841	6.24631275211647
H	1.01891762210956	-1.03914852039815	5.71905758594148
H	1.53730481922609	0.69854604555113	8.56064736728660
H	4.38990551982294	-3.80734521929851	6.83912194789491
H	7.43195376849822	-2.31021655457043	7.55211816359517
H	8.94059026039076	-3.45818019398654	3.31721637166693
H	5.85806217339354	-4.78083524956310	2.54963602360411

Table B13. Cartesian coordinates and total energy in a.u. for RI-BP86/TZVPP of *gc*-**THF<sub>TS</sub>**,  
E(RI-BP86/TZVPP) = -630.7050827698

C	5.03636002460751	0.85842327235752	-2.68967834094463
C	3.23940216150404	-0.60980005261734	-1.33872228105317
C	0.57234178624712	0.27257748585671	-0.90215040173351
C	0.48522883134781	2.18791116399895	1.29435057199021
C	1.95429013325605	1.04704534599082	3.50480772390175
C	2.78456334235551	2.93995326015508	5.50339266322809
O	4.90713345216258	4.33261998273474	4.50734414682875
Ru	7.12265178354886	2.28249536883363	2.57934687705743
O	6.85812447271373	2.80365661264901	-0.74850375466023
O	4.29990374613697	-0.02020520875435	2.48214929507499
O	9.86785246713088	1.50140678505765	3.99666718206448
H	0.90655698590683	-0.54925482499569	4.33861551612876
H	1.29013004415736	4.31845141081517	5.95422149990568
H	3.32781541748101	1.95260370771214	7.25507955482930
H	-1.47262220960916	2.62331591618733	1.84335504497132
H	1.39242242141200	3.97180912218381	0.72950852710814
H	3.65163750466603	-2.60200176066377	-1.03716682039363
H	-0.64994801912211	-1.34874249946661	-0.46244619149174
H	-0.18462775775944	1.16659126230854	-2.62413239659317
H	6.56219405112816	-0.17864610901694	-3.60609988986121
H	4.28053360050427	2.40082770528841	-3.83596436125545

Table B14. Cartesian coordinates and total energy in a.u. for B3LYP/TZVPP of *gc*-**THF**<sub>TS</sub>,

$$E(\text{B3LYP/TZVPP}) = -630.1812048287$$

C	4.99738612615241	0.81797964207950	-2.75426931164229
C	3.22872277202745	-0.60885328486638	-1.38921746633751
C	0.57486494134870	0.27453593140658	-0.90561871795144
C	0.49775368114963	2.16949729724409	1.30273508738019
C	1.98119946285407	1.04468757033512	3.50821888578686
C	2.79449050264193	2.95785611281674	5.49657124639708
O	4.91149936175835	4.32412313543771	4.52506076797391
Ru	7.11402196798420	2.28056697227726	2.58294758691466
O	6.86035894750680	2.85920756644700	-0.69474243881312
O	4.29686837701337	-0.00530853001163	2.49677657775753
O	9.81367056338639	1.45034248334058	4.00536114266539
H	0.93406426903673	-0.52499882095303	4.35429080835288
H	1.29966087358581	4.32046651153373	5.92330610115768
H	3.31013845385888	1.98438441962307	7.24675390059232
H	-1.44740079125776	2.58023000733754	1.85839165997203
H	1.37375343321653	3.95044597047313	0.73767160365915
H	3.65028737934720	-2.57348246539646	-1.03342481989310
H	-0.62864924974445	-1.34289187995463	-0.46928397155617
H	-0.19542835511498	1.17362461760021	-2.59930478525566
H	6.56632126676046	-0.17873188491670	-3.59924421729883
H	4.29836025626429	2.39735657476139	-3.84900547475946

Table B15. Cartesian coordinates and total energy in a.u. for RI-BP86/TZVPP of *at*-**THF<sub>TS</sub>**,

$$E(\text{RI-BP86/TZVPP}) = -630.6901443167$$

C	5.52522887500086	1.95439545084021	1.38598667756954
O	6.50622958287100	5.32917633471709	0.88159635567466
Ru	7.41546045675586	6.22822314698083	-2.21707839274879
O	5.74874149771509	3.23146669189839	-3.42826521601559
C	3.12447157924930	3.87850704586975	-4.05605749685005
C	3.48065106186719	6.08867002865021	-5.83863756350025
O	4.93867426354947	7.84852393893981	-4.32096070528083
C	5.12382306181142	0.66756309794351	-0.93993603985472
C	2.51679610644994	-0.04153502288545	-1.92561245419682
C	1.96825208262992	1.29699581615018	-4.49387671389751
O	10.42176698309041	7.01140428143305	-2.94755558869571
H	-0.06899224851402	1.37930750015349	-4.87880319928454
H	2.90389125796886	0.32839297534620	-6.07374588423516
H	2.22667449970711	4.69507314003560	-2.35368697266617
H	4.49239209667619	5.54390618782402	-7.57604098717441
H	1.69174234381095	7.02625150389170	-6.33657486627878
H	7.21282387459964	1.48201788035099	2.46167125295219
H	3.87645758973607	2.43259706223422	2.52402114364597
H	6.68532747556549	-0.47895323270073	-1.64510081226885
H	2.38056699796551	-2.10446908853638	-2.12655399893559
H	1.07519228711056	0.54022399767857	-0.54675372374972

Table B16. Cartesian coordinates and total energy in a.u. for B3LYP/TZVPP of *at*-**THF<sub>TS</sub>**,

$$E(\text{B3LYP/TZVPP}) = -630.1648046421$$

C	5.50052667218634	1.88269093984754	1.40796283755681
O	6.50572111895855	5.40319130027540	0.85515143427807
Ru	7.40058791095944	6.24379830060185	-2.22305793488349
O	5.75962804316548	3.25498360373025	-3.42696675083491
C	3.16442110321350	3.87915244911564	-4.04979044878501
C	3.47679660031082	6.09786118741151	-5.82605963448046
O	4.93715138400573	7.84869592893097	-4.34355973720593
C	5.10350832523143	0.61944955014776	-0.89541539066490
C	2.51046652995562	-0.04270842636157	-1.92807880816816
C	2.00186282651233	1.30787369219679	-4.49162591686021
O	10.38331786560078	6.97134223098943	-3.00103982698366
H	-0.01764033953587	1.40014505017739	-4.88992168811704
H	2.93741426980200	0.33949714173081	-6.05225511076885
H	2.26133213634678	4.68036586226245	-2.36324588692079
H	4.45894405841097	5.56829532785853	-7.56674601399580
H	1.68243300336128	7.00499610515046	-6.29663746749925
H	7.20972875370650	1.49616899659186	2.45048978302919
H	3.88327597289820	2.42557656377582	2.52955740564924
H	6.65786777017292	-0.49106312705839	-1.62464947184331
H	2.36244548771604	-2.08897995916754	-2.14197242237722
H	1.06638223263803	0.53640601860836	-0.57410413591547

Table B17. Cartesian coordinates and total energy in a.u. for RI-BP86/TZVPP of *gc*-**THP<sub>TS</sub>**,  
 $E(\text{RI-BP86/TZVPP}) = -669.9978049138$

C	5.18844548098727	-2.67994467703565	0.46335937281850
C	2.60121783439499	-2.46724110920155	1.12957833083882
C	0.43665545138201	-2.48854857974997	-0.69612644577269
C	0.76225760618690	-0.82795329940341	-3.06798282377932
C	1.70268510293347	1.87552120195276	-2.51883431549998
C	1.00351860872977	2.90247990615961	0.09470585489914
C	1.96081431118992	5.57901697283063	0.52581396352106
O	4.66077778125080	5.42494908499173	0.88718925159823
Ru	5.60070591349727	2.61049120875564	2.89502608728007
O	6.94329674026221	0.01885909275028	1.19200013743502
O	2.23610027699105	1.41496186299144	2.10913430138668
O	6.48390368105469	3.31792643226784	5.87207332194472
H	-1.04448698808676	2.76114920578124	0.44801470423219
H	1.61646188396334	6.81385377206844	-1.11566307477191
H	1.05187377342014	6.42181809664942	2.19926956354749
H	0.93908134177594	3.17856629954458	-3.94876132759974
H	3.77100742923180	1.97745448996132	-2.68697679567743
H	2.06996531605982	-1.74156357334552	-4.39926156253483
H	-1.07551864918279	-0.76203791697910	-4.03680428766777
H	-1.27956024597005	-1.92077412736669	0.33192786644677
H	0.08192930198862	-4.45491647365884	-1.30459688630056
H	2.11878522454388	-2.89548216750256	3.08631161759737
H	6.31512200940966	-3.93463146231726	1.64916143005876
H	5.64762441045615	-2.80797345850773	-1.54406382698233

Table B18. Cartesian coordinates and total energy in a.u. for B3LYP/TZVPP of *gc*-**THP<sub>TS</sub>**,  
E(B3LYP/TZVPP)= -669.4443884176

C	5.17731019003031	-2.76363504263726	0.45484156983888
C	2.62104879787572	-2.53506641014114	1.10726133065175
C	0.44610465348414	-2.49694849987536	-0.69877014970220
C	0.75468071919232	-0.81765619023838	-3.05198490993766
C	1.68714913876507	1.88489662205766	-2.51082675985565
C	1.01643323567110	2.91561780251794	0.10606048459680
C	1.98689669931196	5.59116011088017	0.51680982338070
O	4.65665136005359	5.43500641057736	0.90112313007495
Ru	5.58232516686540	2.60840947268354	2.88951057729599
O	6.95584516002846	0.08498819929627	1.18573979228615
O	2.23295380403695	1.43189526662746	2.08142503489465
O	6.38596404573716	3.29254556077695	5.86850669075692
H	-1.01890615603548	2.80332418090343	0.45135952654887
H	1.64680716680280	6.80376612238419	-1.12217980820050
H	1.06978971668414	6.44010421243898	2.16433562357124
H	0.90252907128625	3.16961914916996	-3.92365651721405
H	3.73633451090191	1.98910805659761	-2.70936842591045
H	2.04347242096899	-1.71413381069431	-4.39022969177244
H	-1.08000008453336	-0.75354194937246	-3.99518825074559
H	-1.23827080730056	-1.92602465283274	0.34711151339695
H	0.07353802755028	-4.43878708980430	-1.32182718228790
H	2.13574854515466	-2.92267852444334	3.05482874348631
H	6.34140665994942	-3.90572366787953	1.68472724800158
H	5.67685155398901	-2.86026454735600	-1.52511493613699

Table B19. Cartesian coordinates and total energy in a.u. for RI-BP86/TZVPP of *at*-**THP<sub>TS</sub>**,  
E(RI-BP86/TZVPP)= -669.9990472518

C	7.03352668984213	-0.31554666944895	0.39213468833878
O	8.41423576511331	0.89781568628526	3.21066341351099
Ru	6.55311591483905	2.64117980279506	5.40992046967085
O	3.52777778142087	1.24700511157020	3.91327689148292
C	2.60010918895861	-0.91276773080710	5.39381552510139
C	2.88293136695817	-0.04780126736654	8.10758731988267
O	5.45367942870538	0.84422874960921	8.32657277257219
C	4.36182903450331	-0.10387937551344	0.33936910679901
C	2.59478895745898	-2.32596974448592	0.27870964591762
C	-0.01334408725768	-1.77618135090385	1.46146855550251
C	0.00805452627094	-1.63838498927580	4.38659858994276
O	6.93879359980408	5.77261802686981	5.86794499095235
H	3.93556224214890	-2.49131569514897	5.11731642418846
H	1.52037286583141	1.46617217505276	8.55569184040436
H	2.64023605167587	-1.60411840690965	9.46848083882656
H	-1.41733828899361	-0.27463591701319	5.04136052086686
H	-0.49893246356453	-3.48518574614972	5.19810912394244
H	-1.37295570832488	-3.21927484798158	0.84571609490531
H	-0.69282219771721	0.03028585040373	0.69221526103022
H	3.48865332558962	-3.99557277622332	1.14280551040713
H	2.30658558063967	-2.82847787885747	-1.72757493764092
H	3.57383794492537	1.65223461374817	-0.40194196821026
H	8.07984207075810	0.95451054255463	-0.84675817407668
H	7.82481051087262	-2.21745456216284	0.51089586265863

Table B20. Cartesian coordinates and total energy in a.u. for B3LYP/TZVPP of *at*-**THP<sub>TS</sub>**,  
E(B3LYP/TZVPP)= -669.4457592240

C	7.01476177679816	-0.33846025360670	0.31340933031413
O	8.42207374142897	0.87128247055845	3.29422780361079
Ru	6.54828830718456	2.61688886265304	5.41942961077590
O	3.53460396728284	1.23515737066462	3.92993312819129
C	2.60699253937302	-0.88915160441866	5.39775148885337
C	2.88323688687453	-0.04033000670046	8.11586667404733
O	5.42471384089526	0.85786271289101	8.34368803067638
C	4.37412803466952	-0.12736394073575	0.28133660883202
C	2.59091879596791	-2.33164275252208	0.27111237050290
C	0.00134402716067	-1.76496473420329	1.47365464954299
C	0.02442468727956	-1.62756462642775	4.39277966912936
O	6.87751008439593	5.73546233445619	5.84044349803961
H	3.92486383727949	-2.46373231154313	5.13441647385292
H	1.52204036714368	1.45355509837183	8.56457482477281
H	2.63329599833802	-1.59675427554739	9.45186469696210
H	-1.39998272853649	-0.28015801654660	5.03666572507335
H	-0.47159266261396	-3.46396276532211	5.19705306738427
H	-1.35540988833531	-3.19439950671043	0.86898109943663
H	-0.67096798645951	0.02989002227036	0.71137293080108
H	3.48046787900188	-3.98732007788130	1.12830502353072
H	2.27990207462761	-2.83595296861687	-1.71521061443565
H	3.58311218007070	1.62673196793961	-0.41378841463859
H	8.08119341310754	0.99090946457094	-0.81004169312617
H	7.83343092752392	-2.20649886295306	0.45655238484660

## References

- [1] R. Ahlrichs, M. Bär, M. Häser, H. Horn, C. Kölmel, *Chem. Phys. Lett.* **1989**, *162*, 165–169.
- [2] J. P. Perdew, *Phys. Rev. B* **1986**, *33*, 8822–8824.
- [3] A. D. Becke, *Phys. Rev. A* **1988**, *38*, 3098–3100.
- [4] E. J. Baerends, D. E. Ellis, P. Ros, *Chem. Phys.* **1973**, *2*, 41–51.
- [5] B. I. Dunlap, J. W. D. Connolly, J. R. Sabin, *J. Chem. Phys.* **1979**, *71*, 3396–3402.
- [6] F. Weigend, *Phys. Chem. Chem. Phys.* **2006**, *8*, 1057–1065.
- [7] C. Lee, W. Yang, R. G. Parr, *Phys. Rev. B* **1988**, *37*, 785–789.
- [8] A. D. Becke, *J. Chem. Phys.* **1993**, *98*, 5648–5652.
- [9] F. Weigend, R. Ahlrichs, *Phys. Chem. Chem. Phys.* **2005**, *7*, 3297–3305.
- [10] D. Andrae, U. Häußermann, M. Dolg, H. Stoll, H. Preuß, *Theor. Chim. Acta* **1990**, *77*, 123–141.